

## Combined Effect of Pore Radius and Protein Dielectric Coefficient on the Selectivity of a Calcium Channel

Dezso Boda,<sup>1,2,\*</sup> Mónika Valiskó,<sup>2</sup> Bob Eisenberg,<sup>1</sup> Wolfgang Nonner,<sup>3</sup> Douglas Henderson,<sup>4</sup> and Dirk Gillespie<sup>1</sup>

<sup>1</sup>*Department of Molecular Biophysics and Physiology, Rush University Medical Center, Chicago, Illinois 60612, USA*

<sup>2</sup>*Department of Physical Chemistry, University of Pannonia, P. O. Box 158, H-8201 Veszprém, Hungary*

<sup>3</sup>*Department of Physiology and Biophysics, University of Miami School of Medicine, Miami, Florida 33101, USA*

<sup>4</sup>*Department of Chemistry and Biochemistry, Brigham Young University, Provo, Utah 84602, USA*

(Received 28 August 2006; published 17 April 2007)

Calcium-selective ion channels often contain a selectivity filter made of similar amino acids, rich in carboxylates, although the  $\text{Ca}^{2+}$  affinities of these channels range from micromolar to millimolar. To understand the physical mechanism for this range of affinities, we use grand canonical Monte Carlo simulations to study the competition of  $\text{Na}^+$  and  $\text{Ca}^{2+}$  in the selectivity filter of a reduced model of a Ca channel. We show that  $\text{Ca}^{2+}$  affinity is increased dramatically when both the volume and dielectric coefficient of the protein are reduced.

DOI: [10.1103/PhysRevLett.98.168102](https://doi.org/10.1103/PhysRevLett.98.168102)

PACS numbers: 87.15.Kg

The physical mechanism by which genetic information controls the ion-binding properties of proteins is an important topic in molecular biophysics. Here, we show that the pores of  $\text{Ca}^{2+}$ -selective ion channels can bind  $\text{Ca}^{2+}$  with a range of specificities set by two parameters (the radius of the pore and the dielectric coefficient of the protein) that characterize our low-resolution model. This model can also describe  $\text{Ca}^{2+}$ -binding pockets in many other proteins. We vary the radius of the pore to change the packing fraction of groups directly involved in coordinating  $\text{Ca}^{2+}$  ions. The packing fraction is a low-resolution parameter because our model does not include any specification of the exact positions of these coordinating atoms [1,2]). We also vary the dielectric coefficient of the protein material that is near the coordinating groups. Proteins can implement complex polarization properties by allowing different movements of their many kinds of electric charge—permanent and induced—in their backbone and in amino acid residues. In genetic terms, our parameters constitute phenotypes that might result from a variety of genetically encoded, specific atomic structures of protein. Identifying such parameters is also a first step in engineering of the protein.

Calcium ions enter the cytosol through Ca channels (e.g., the *L*-type and ryanodine receptor, RyR, Ca channels) and then activate many proteins.  $\text{Ca}^{2+}$  transduces a signal from an extracellular receptor into intracellular protein function. The selectivity filters of Ca channels preferentially accumulate  $\text{Ca}^{2+}$  over monovalent cations even though the monovalent cations are present at much higher concentrations. For example, in single channel current-voltage experiments with 100 mM bath  $\text{Na}^+$  concentration, a few  $\mu\text{M}$   $\text{Ca}^{2+}$  blocks  $\text{Na}^+$  current in the *L*-type Ca channel, while it takes a thousand times as much  $\text{Ca}^{2+}$  (in the millimolar range) to have the same effect in the RyR channel. The different selectivity behavior of these channels is evolutionarily correlated with their different physi-

ological functions. Despite their different  $\text{Ca}^{2+}$  affinities, the *L*-type and RyR Ca channels have a common structural motif of four glutamate (Glu) or Aspartate (Asp) amino acids in their selectivity filters [1,2]. Their groups make the selectivity filter a negatively charged, carboxylate-rich site. Carboxylate-rich pockets are also present in many other proteins (e.g., proteins containing the EF-hand motif [3]), where they can bind  $\text{Ca}^{2+}$  with a wide range of affinities.

Ion conduction in *L*-type Ca channels has been modeled in molecular dynamics (MD) [4] and Brownian dynamics (BD) [5]. The BD simulations suggested that the main driving force for divalent vs monovalent selectivity is electrostatics [6], while other work has suggested that it is the balance of electrostatics with excluded volume in the crowded selectivity filter (the charge-space competition, CSC, model) [7,8]. Others have shown selectivity arising from excluded volume alone in narrow pores [9]. Early MD and BD simulations were restricted to conditions of large ion concentrations and strong electric fields. The low  $\text{Ca}^{2+}$  concentrations of biological interest were not modeled. In later work we showed that Ca channels can be modeled in low  $\text{Ca}^{2+}$  concentrations using Monte Carlo (MC) simulation and the grand canonical (GC) ensemble [10]. As far as we know, these are the first particle simulations of  $\text{Ca}^{2+}$ -protein interactions at the low  $\text{Ca}^{2+}$  concentrations at which they normally function. Here we show that pore radius and dielectric environment together can tune  $\text{Ca}^{2+}$  affinity on a broad scale, from 1 mM (1000  $\mu\text{M}$ ) to 0.03 mM (30  $\mu\text{M}$ ), and that together the radius and dielectric coefficient produce a much larger effect than they do individually.

A cylindrical simulation cell is subdivided into two bath compartments by a membrane that contains a protein with a pore through it [Fig. 1(a)]. These domains have hard boundaries impenetrable to ions. The protein (but not the pore) is assigned a dielectric coefficient that is either  $\epsilon = 80$  (i.e., waterlike) or  $\epsilon = 10$ . The dielectric coefficient in

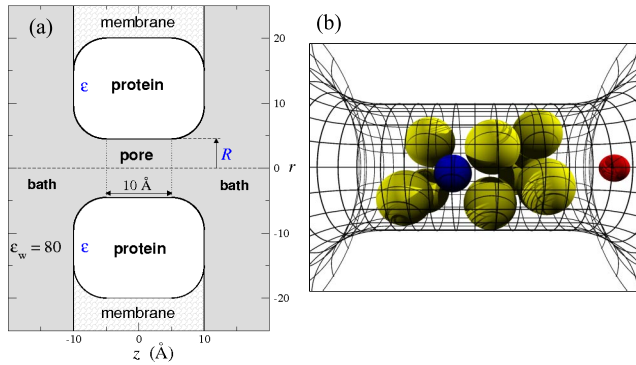


FIG. 1 (color online). (a) Geometry of the simulated Ca channel. This cross section shows the central part of the cylindrical simulation cell (typically 75 Å in radius and 320 Å in length). (b) Snapshot from a simulation: ions in the pore (large yellow:  $O^{1/2-}$ ; small blue in the center:  $Ca^{2+}$ ; small red at the entrance:  $Na^{+}$ ).

the rest of the simulation cell (including the pore) is always  $\epsilon_w = 80$ . A dielectric coefficient of  $\epsilon_w = 80$  is used also for the membrane in order to reduce computation time for the electrostatics, but this does not affect the final results [10]. The electrolyte is represented in the primitive model, as hard-sphere ions with central charges. Ionic radii are 1, 0.99, and 1.81 Å for  $Na^{+}$ ,  $Ca^{2+}$ , and  $Cl^{-}$ , respectively. (The existing uncertainty whether to use Pauling or Born radii in continuum solvent models must be resolved with simulations using explicit water. [11].) The dimensions of the simulation cell are large enough to allow the formation of bulklike solutions in both baths.

A snapshot from a simulation illustrates our reduced model of the central part of the pore that contains the charged  $COO^{-}$  groups of the protein's amino acids that extend into the ionic pathway [Fig. 1(b)]. These groups are modeled here as distinct half charged oxygen ions ( $O^{1/2-}$ , radius 1.4 Å) that are restricted to the central cylinder of the pore so that they cannot overlap the cylinder boundaries. These oxygen particles act like free ions, except for their confinement. The radius of the confining central cylinder is varied between  $R = 3.5$  and  $R = 5$  Å, while the length of the cylinder is fixed at 10 Å.

We simulate a mixed thermodynamic ensemble where temperature ( $T = 298.15$  K), cell volume, and the number of  $Na^{+}$  particles (300 in most runs) are fixed. The length and radius of the simulation cell are chosen so that the number of  $Na^{+}$  yields a bath concentration of 0.1 M.  $Ca^{2+}$  and  $Cl^{-}$  particles are simulated in the GC ensemble by simultaneously inserting or deleting 1  $Ca^{2+}$  and 2  $Cl^{-}$  while maintaining a fixed chemical potential for  $CaCl_2$ . The  $Ca^{2+}$  concentrations in the baths are outputs of the simulations. The particle insertion or deletion step is coupled to a biased particle exchange between the channel and the bath to accelerate the convergence of the average number of  $Ca^{2+}$  and  $Na^{+}$  ions in the channel [10,12]. The

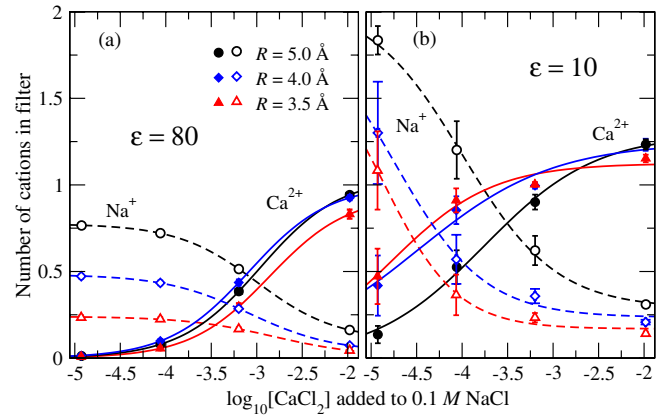


FIG. 2 (color online). Occupancy curves: the average numbers of  $Na^{+}$  and  $Ca^{2+}$  ions in the pore (occupancy) vs the logarithm of  $CaCl_2$  concentration in the bath ( $[NaCl] = 0.1$  M). The symbols are simulation results; the curves are fitted using Eq. 7 of Ref. [8]; the fit includes a point obtained from a canonical MC simulation in the absence of  $CaCl_2$  (not shown). Solid and dashed lines refer to  $Ca^{2+}$  and  $Na^{+}$  ions, respectively.

electrostatic energy of the system is determined using the Induced charge computation (ICC) method [10,13], which numerically solves an integral equation for the surface charge induced on dielectric boundaries. The ICC method gives accurate results even for curved boundaries.

The affinity of the channel for each ionic species is characterized by its occupancy: the average number of  $Ca^{2+}$  and  $Na^{+}$  ions located in the cylindrical pore ( $|z| \leq 5$  Å).  $Ca^{2+}$  and  $Na^{+}$  occupancies are plotted as functions of  $\log_{10}[CaCl_2]$  in the bath in Fig. 2. The figure shows that  $Ca^{2+}$  replaces  $Na^{+}$  in the filter as the bath  $Ca^{2+}$  concentration increases. We characterize the selectivity of the channel by the  $[CaCl_2]$  at which the numbers of  $Ca^{2+}$  and  $Na^{+}$  in the filter are equal (i.e., the  $[CaCl_2]$  where the  $Ca^{2+}$  and  $Na^{+}$  curves in Fig. 2 intersect). The smaller this  $[CaCl_2]$ , the more selective the channel is for  $Ca^{2+}$  over  $Na^{+}$ . We plot this characteristic concentration as a function of  $R$  in Fig. 3.

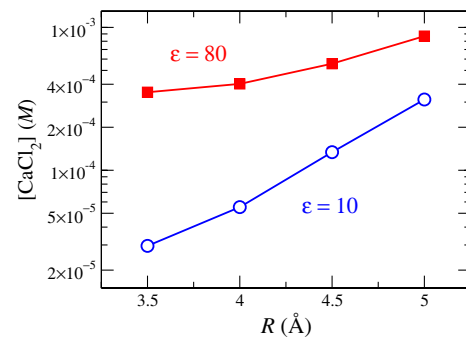


FIG. 3 (color online). The  $[CaCl_2]$  where the occupancy curves for  $Ca^{2+}$  and  $Na^{+}$  of Fig. 2 intersect, as a function of the radius of the pore.

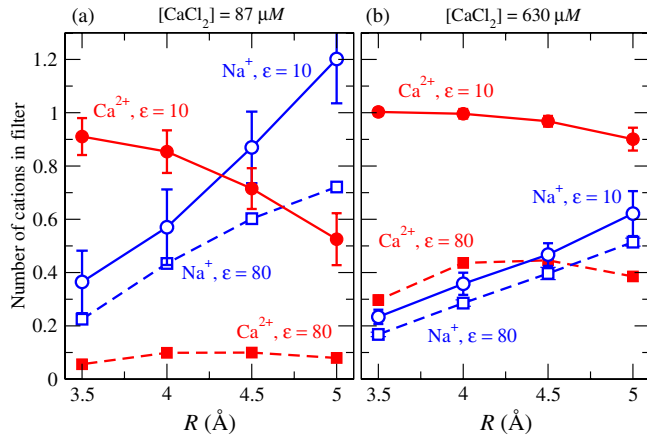


FIG. 4 (color online). Occupancy curves: the average number of  $\text{Ca}^{2+}$  and  $\text{Na}^+$  ions in the pore as a function of  $R$  for  $\epsilon = 10$  and 80 at two fixed  $[\text{CaCl}_2]$ .

The figure shows that for a given radius  $\text{Ca}^{2+}$  vs  $\text{Na}^+$  selectivity increases considerably when we reduce  $\epsilon$  from 80 (squares) to 10 (circles). In the case of  $\epsilon = 10$  more positive charge is attracted into the filter so that less negative polarization charge is induced on the wall of the pore (in the  $\epsilon = 80$  case these induced charges are absent) [10]. This increased ionic density results in an increased hard-sphere repulsion. The competition of these two effects results in a better  $\text{Ca}^{2+}$  vs  $\text{Na}^+$  selectivity as  $\epsilon$  decreases. Because of hard-sphere exclusion, the pore is not electroneutral in our simulations; the structural charge of the pore is screened by counterions nearby in the vestibules and baths rather than by counterions in the pore itself (discussed later).

Figure 3 also shows that  $\text{Ca}^{2+}$  vs  $\text{Na}^+$  selectivity increases only about twofold as the pore radius is reduced in the case of  $\epsilon = 80$  (squares); it increases much more (about 12-fold) in the case of  $\epsilon = 10$  (circles). To gain an insight into this behavior, we consider the total numbers of  $\text{Na}^+$  and  $\text{Ca}^{2+}$  ions as functions of  $R$  for  $[\text{CaCl}_2] = 87$  and  $630 \mu\text{M}$  in Fig. 4. In the case of  $\epsilon = 80$ , the number of  $\text{Na}^+$  in the pore becomes smaller as the size of the filter decreases, while the number of  $\text{Ca}^{2+}$  changes less (squares with dashed lines). For this reason, decreasing  $R$  increases  $\text{Ca}^{2+}$  vs  $\text{Na}^+$  affinity, but only moderately. In the case of  $\epsilon = 10$ , the number of  $\text{Na}^+$  still decreases with decreasing  $R$ , but now the number of  $\text{Ca}^{2+}$  increases (circles with solid lines). As a consequence, better  $\text{Ca}^{2+}$  vs  $\text{Na}^+$  selectivity is produced *both* by decreasing the amount of  $\text{Na}^+$  in the filter with decreasing  $R$ , *and* by increasing the number of  $\text{Ca}^{2+}$  (Fig. 5). The excluded  $\text{Na}^+$  ions accumulate at the entrances of the pore just outside the domain accessible to the  $\text{O}^{1/2-}$  ions where they contribute to the neutralization of the negative pore. This behavior becomes more pronounced with decreasing  $R$ .

To examine the interplay between excluded volume and electrostatics, we consider the total number of cations

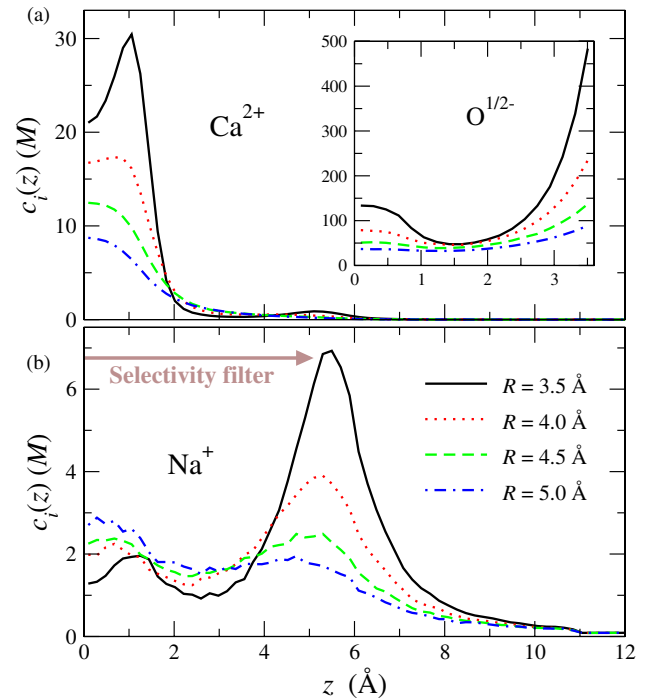


FIG. 5 (color online). Longitudinal profiles for (a)  $\text{Ca}^{2+}$  ( $\text{O}^{1/2-}$ , inset) and (b)  $\text{Na}^+$  ions in the pore for different pore radii,  $\epsilon = 10$  and  $[\text{CaCl}_2] = 630 \mu\text{M}$ . The concentration profiles are averages over the cross section of the simulation cell.

$N_{\text{cation}}$  [Fig. 6(a)] and the total number of cationic charges  $Q_{\text{cation}}$  [Fig. 6(b)] in the pore as functions of  $R$ .  $N_{\text{cation}}$  decreases with decreasing  $R$  [Fig. 6(a)] in every case because less space is available in the pore. Ionic densities become very high in the pore as  $R$  decreases (Fig. 5) and the CSC mechanism favors  $\text{Ca}^{2+}$  ions in narrower channels (Fig. 3) because  $\text{Ca}^{2+}$  provides twice the positive charge that  $\text{Na}^+$  does in the same ionic volume to balance the negative charge of the oxygens. In the case of  $\epsilon = 80$ ,  $Q_{\text{cation}}$  decreases as  $R$  decreases because more counterions (primarily  $\text{Na}^+$ ) are squeezed out of the pore. The electro-

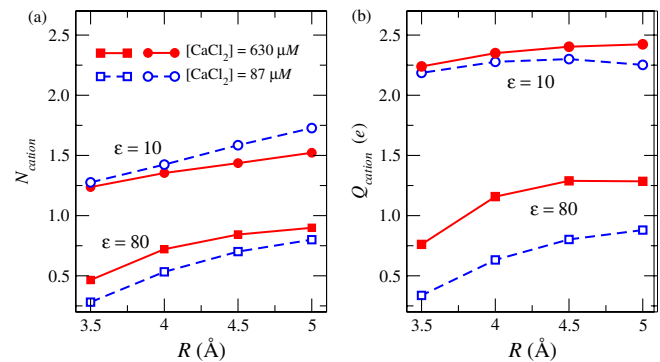


FIG. 6 (color online). (a) Total number of cations  $N_{\text{cation}}$  and (b) total charge of cations  $Q_{\text{cation}}$  in the pore as functions of  $R$  for  $\epsilon = 10$  and 80 at two fixed  $\text{CaCl}_2$  concentrations.  $Q_{\text{cation}} = 4$  would be perfect charge neutrality in the pore.

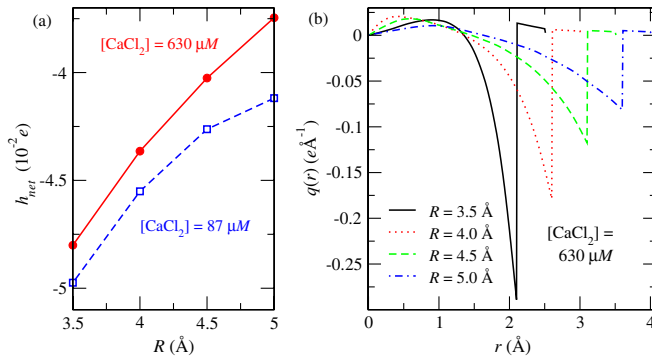


FIG. 7 (color online). (a) Total induced charge  $h_{\text{net}}$  on the cylindrical wall of the pore as a function of  $R$  for  $\epsilon = 10$  at two bath  $\text{CaCl}_2$  concentrations. For  $\epsilon = 80$  the induced charge is zero. (b) The radial ionic charge profile in the pore averaged over the axial dimension,  $\epsilon = 10$  and  $[\text{CaCl}_2] = 630 \mu\text{M}$ .

static attraction provided by the oxygen ions is not enough to balance the increasing hard-sphere exclusion.

In the case of  $\epsilon = 10$ , the net cationic charge  $Q_{\text{cation}}$  is quite unaffected as  $R$  decreases [Fig. 6(b)]. Apparently, the electrostatics of a pore embedded in a weak dielectric is strong enough to keep *countercharge* in the pore even as the pore radius is reduced and *counterions* are squeezed out.  $Q_{\text{cation}}$  can be kept at a certain level [Fig. 6(b)] while, at the same time,  $N_{\text{cation}}$  is decreased only if  $\text{Na}^+$  is exchanged for  $\text{Ca}^{2+}$  as shown in Fig. 4. Because of this cation exchange we obtain better improvement in  $\text{Ca}^{2+}$  vs  $\text{Na}^+$  selectivity with decreasing  $R$  in the case of  $\epsilon = 10$  than in the case of  $\epsilon = 80$ .

One reason for the ion exchange is the ability of the low dielectric pore to maintain the level of local electroneutrality even if the radius of the pore is decreased. Insight can be gained by considering the average negative induced polarization charge that is determined by the average structure of the ions inside the pore. Figure 7(a) shows that the average induced charge on the wall of the pore becomes more negative as  $R$  decreases. Figure 7(b) shows that near the pore wall the ionic charge is negative, i.e., dominated by the oxygen ions whose fixed number is confined into a smaller space. Figure 5 indicates that along the  $z$  axis the oxygen ions concentrate mostly near the mouths of the pore. This distribution of oxygen ions forms a pocket of negative charge around the cations in the pore center (mostly  $\text{Ca}^{2+}$ ).

The increase in negative ionic charge density at the wall produces more negative induced charge on this wall. This average induced charge is small compared to the net ionic charge in the pore, although instantaneously it might be locally large as individual ions move. Induced charge is a separation of charge on the surface and that separation requires energy that is a large component of the free energy of the system. Increasing the cation concentration in the pore reduces both the net ionic charge in the pore and the induced charge on the pore wall (both are negative), and

thus reduces the electrostatic energy of the system. This reduction in the electrostatic component of the free energy balances the increasing entropic (excluded volume) component that results from the increase in ionic density. The net result is that the induced charge amplifies the attractive effect of the oxygen ions, but in a complicated, nonadditive manner.

In conclusion, the increased  $\text{Ca}^{2+}$  selectivity of the channel is the result of two mechanisms: (1) decreasing the pore radius  $R$  increases ionic density which, in turn, excludes  $\text{Na}^+$  from the pore; (2) decreasing the protein dielectric coefficient  $\epsilon$  increases the number of cations in the pore and produces a constant cationic charge in the pore that does not change as  $R$  decreases. Simultaneously decreasing both  $R$  and  $\epsilon$  changes “ $\text{Ca}^{2+}$  over  $\text{Na}^+$  selectivity-ratio” 30-fold, from 100:1 to 3000:1. The apparent dissociation constant of  $\text{Ca}^{2+}$  in the presence of 0.1 M  $\text{Na}^+$  is reduced from 1 mM to 30  $\mu\text{M}$ . Any (evolutionary or engineered) changes to the Ca channel protein that specifically modify these two low-resolution parameters can thus tune the ionic selectivity over a fairly wide range.

The authors thank the Ira and Marylou Fulton Supercomputing Center at BYU, the Hungarian National Research Fund (OTKA No. K63322), NATO Grant No. PST.CLG.980366, and NIH Grant No. GM067241.

\*Corresponding author.

Electronic address: dezso\_boda@rush.edu

- [1] J. Yang, P. T. Ellinor, W. A. Sather, J. F. Zhang, and R. W. Tsien, *Nature (London)* **366**, 158 (1993).
- [2] L. Gao, D. Balshaw, L. Xu, A. Tripathy, C. Xin, and G. Meissner, *Biophys. J.* **79**, 828 (2000).
- [3] M. R. Nelson and W. J. Chazin, *Biometals: Int. J. Metal Ions Biol., Biochem., Med.* **11**, 297 (1998).
- [4] Y. Yang, D. Henderson, and D. Busath, *J. Chem. Phys.* **118**, 4213 (2003).
- [5] B. Corry, T. W. Allen, S. Kuyucak, and S.-H. Chung, *Biophys. J.* **80**, 195 (2001).
- [6] B. Corry, T. Vora, and S.-H. Chung, *Biochim. Biophys. Acta* **1711**, 72 (2005).
- [7] W. Nonner, L. Catacuzzeno, and B. Eisenberg, *Biophys. J.* **79**, 1976 (2000).
- [8] D. Boda, D. D. Busath, D. Henderson, and S. Sokolowski, *J. Phys. Chem. B* **104**, 8903 (2000).
- [9] D. Goulding, J.-P. Hansen, and S. Melchionna, *Phys. Rev. Lett.* **85**, 1132 (2000).
- [10] D. Boda, M. Valiskó, B. Eisenberg, W. Nonner, D. Henderson, and D. Gillespie, *J. Chem. Phys.* **125**, 034901 (2006).
- [11] J. Dzubiella, R. J. Allen, and J.-P. Hansen, *J. Chem. Phys.* **120**, 5001 (2004).
- [12] D. Boda, D. Henderson, and D. D. Busath, *Mol. Phys.* **100**, 2361 (2002).
- [13] D. Boda, D. Gillespie, W. Nonner, D. Henderson, and B. Eisenberg, *Phys. Rev. E* **69**, 046702 (2004).